Numerical Modeling and Laboratory Validation of Geosynthetic Stabilized Structures

Lois G. Schwarz and Mark H. Wayne
Tensar International, Alpharetta, GA, USA

ABSTRACT
Predicting the effective use of geosynthetics in composite systems requires an understanding of its performance in combination with the characteristics of the surrounding unbound materials. This paper explicates the importance of validating finite element calculations as they relate to geosynthetic mechanically stabilized structures by comparing results from basic large-scale laboratory type plate load testing. Numerical modeling includes a control structure without geogrid, a structure using a traditional geogrid element, and a structure using a new TSSM model based on composite material behavior. The TSSM composite material represents both the geogrid and soil interface that expands the soil-structure interaction behavior beyond using a typical planar membrane type geogrid structure element with interface elements placed between the membrane element and the soil. Our experience and research have shown that the interaction of the geosynthetic and the soil provides more improvement in performance than predicted by the properties of the individual components alone.

RÉSUMÉ
Pour prédire l'utilisation efficace de géosynthétiques dans des systèmes composites, il est nécessaire d'avoir une compréhension de ses performances en combinaison avec les caractéristiques des matériaux non liés environnants. Cet article explique l'importance de la validation des calculs par éléments finis dans la mesure où ils se rapportent à des structures géosynthétiques stabilisées mécaniquement en comparant des résultats d'essais de charge sur plaque à grande échelle en laboratoire. La modélisation numérique comprend une structure de contrôle sans géogrille, une structure utilisant un élément de géogrille traditionnel et une structure utilisant un nouveau modèle TSSM basé sur le comportement du matériau composite. Le matériau composite TSSM représente à la fois la géogrille et l'interface de sol qui étend le comportement d'interaction sol-structure au-delà de l'utilisation d'un élément de structure de géogrille de type membrane plane typique avec des éléments d'interface placés entre l'élément de membrane et le sol. Notre expérience et nos recherches ont montré que l'interaction du géosynthétique et du sol offre une amélioration des performances supérieure à celle prévue par les propriétés individuelles des composants.

1 INTRODUCTION

The role of the finite element method (FEM) has evolved from a research tool into a daily engineering tool, sharing a complementary position next to conventional design methods (Brinkgreve and Engin, 2013). The basic questions to be considered with numerical modeling, as well as with conventional design methods, is how does the ground want to behave and what mechanisms are at work to influence the behavior? The type of geotechnical application using geogrid stabilization or reinforcement dictates which mechanisms will dominate the behavior of soil and should not be lost in the details of calculations.

Geogrids have been increasingly used successfully for soil stabilization during the past 35 years. The benefits of using geogrid to increase bearing capacity and reduce settlement have been well recognized. Commonly referred to as planar material, geogrids are used in roadways to stabilize soft subgrade and granular soil by providing lateral confinement of unbound aggregate. Results of physical performance testing on geogrid stabilized roadways can be divided into plate load tests, moving wheel tests, moving vehicle tests, and composite testing programs. Due to ease of test set-up in a laboratory controlled environment and common equipment involved, numerous researchers have investigated the effects of geogrid by performing plate load tests including Guido et al. (1987), Gabr et al. (1998), Jersey and Tingle (2009), and Dong et al. (2010).

Design of geosynthetic stabilized pavements and working platforms requires proper evaluation of the load-transfer mechanisms between soil particles and geosynthetics. The type of application will designate which mechanism(s) dominate for specific conditions. In the case of stabilized pavements and working platforms, the mechanical response can be dominated by stress redistribution, restriction of lateral spreading, and tension membrane effect (Giroud and Han, 2016a). The level of dominance of each response will depend on the structure and the ground conditions of the application. For example, the tension membrane effect can be the primary load-transfer mechanism for heavy haul roads but is not active for pavements unless severe rutting occurs. Restricting lateral spreading is a major concern for embankments and to some extent raised working platforms for maintaining structural strength but can be a secondary concern for haul roads. Heavy haul roads require stresses to be redistributed in order to be operative and avoid serious rutting problems on weak cohesive soils, and similar needs for stress redistribution may be required for reinforced substructure support of shallow foundations (Giroud and Han, 2016b).

2 GEOGRID MATERIAL PROPERTIES AND MODELING INTRODUCTION

It is well known that biaxial geogrid has been used extensively in highway pavement and railway applications and uniaxial geogrid for retaining wall and slope applications. Numerical models used to characterize biaxial and uniaxial geogrids are based on their strength properties or in-air tensile stiffness and the mechanical characteristics of the soil unaltered by the presence of the geogrid, with a possible exception for interface properties between the two materials (Milligan et al., 1989). This can lead to significant under-prediction of geogrid performance, particularly for multiaxial geogrids whose primary function is stabilization. Furthermore, the stabilizing effect of multiaxial geogrid extends a relatively significant distance from the geogrid plane, typically 300 mm or more (Bussert and Cavanaugh, 2010). Consequently, conventional methods of characterizing the mechanical properties of soil and geogrid separately are not suited to multiaxial stabilizing geogrid that depends critically on the interaction between soil particles and geogrid.

Using incorrect parameters for the geogrid will invariably affect the numerical results and may over-or-under estimate the performance capabilities of the geogrid material. To this point, the authors have found perhaps the most misunderstood and problematic parametric input is designated as axial tension stiffness of the geogrid, referred to as EA, and has units of force per unit length. This parameter is Young's modulus, E (with units of force per square length) of the geogrid multiplied by the cross-sectional area, A (with units of square length), and herein lies the problem. Young's modulus of the geogrid can be determined from in-air tensile testing and resulting stress-strain curves, however what is the area to be used? Using the lateral area of the geogrid, i.e., length multiplied by width, is not correct because geogrid is composed of nodes with intersecting ribs and there is no polymer material in-between these components. The geogrid area per unit length is the product of material width and nominal thickness. Thickness of the geogrid is referred to as a nominal dimension, and must take into account the thickness of the ribs, nodes, and the percent open non-polymer areas. Accordingly, nominal thickness is based on the material weight and density. However, multiaxial geogrids have further complicated the conundrum of determining what is the axial stiffness parameter since Young's modulus is not as easily determined from laboratory testing as uniaxial and biaxial geogrids. Accordingly, multiaxial geogrid requires more intricate means of characterization because its stabilizing effect on soil needs to be characterized more than the mechanical properties of the geogrid itself.

Unlike geotextiles, the physical structure of geogrid has an inherent sizeable percentage of open area between the ribs and nodes. The physical openness of geogrid geometry allows aggregates to penetrate through the plane of the geogrid and lock in place as shown in Figure 1(a) and this penetration enhances interlock and load redistribution. When a force is applied to overlying aggregates, the force becomes transmitted to the geogrid which acts as a restraint as illustrated in Figure 1(b). The mechanism of geogrid interlocking with aggregate is not the same for different geogrids, nor for different soils. Factors which govern geogrid-aggregate interlock include geogrid aperture size relative to aggregate size and grading, geogrid aperture shape, shape and stiffness of geogrid ribs, and junction stiffness between the ribs of the geogrid (Giroud, 2009).

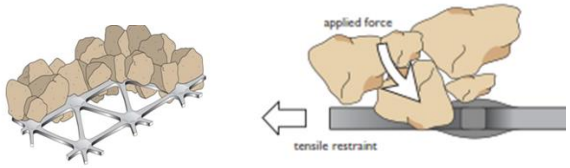

(a) (b)

Figure 1. Open geometry of geogrids showing (a) aggregate penetration, (b) tensile restraint

Obviously, the interlocking of geogrid with aggregate materials creates a unique interface. Interfaces for dissimilar elements in FEM, and in particular the case of geogrid and soil, present a transition zone to model soil-structure interaction with input parameters referenced to the adjacent soil material. This means the interface element strength is related to the shear strength of the contact soil and is typically reduced by a user selected input factor ≤ 1. The thickness of the interface zone can also be input but is limited to a relatively thin zone, typically on the order of one or two mesh elements thick by the software.

To overcome the geogrid structural and mechanistic problems in modeling geogrid and soil materials, the geogrid product and soil can be modeled as a composite material using a recently developed T-Method Stabilized Soil Model (TSSM) designed to be compatible with most commercially available FEM software (Lees, A., 2017a). The "T" in the designation represents load transfer efficiency of the soil.

3 LABORATORY PLATE LOAD TESTING

3.1 Laboratory Testing Materials and Procedures

Two series of in-house laboratory type plate load tests were conducted using a 305 mm diameter steel load plate, hydraulic load frame, and a 1220 mm diameter steel test box filled with aggregate material. The aggregate used in Series-1 testing used a clean limestone ballast material having an elongated shape, rough surface texture, and particle gradation ranging between 60 mm to 10 mm. Series-2 testing used a tempered glass material called fireglass to simulate a smaller-sized natural aggregate with particles sizes of about 18 mm to 2 mm. Tamped thickness of the aggregate layer was nominally 152 mm regardless of the type of aggregate used. Underlying the aggregate material was a layered rubber mat material, having a total thickness of 203 mm, density of 1.628 g/cm^3, and was not of notable interest for this testing program. The mat was placed directly on top of the reinforced concrete laboratory

floor. The rubber mat material and tempered fireglass material were primarily selected to enable easier set-up of the test specimens and to maintain consistency of material properties; similar replacement of natural soil and aggregate materials in laboratory testing is becoming more common. Surface deformation was measured using a laser micrometer mounted on the load frame and referenced to the load plate surface. A schematic of the test set-up is shown in Figure 2.

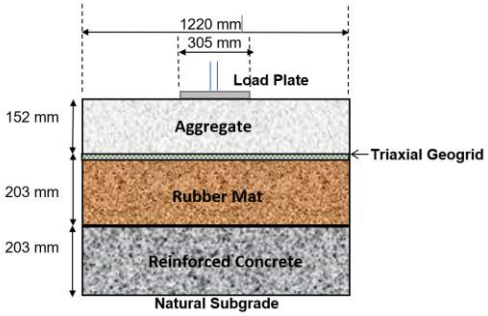

Figure 2. Schematic representation of load test set-up

3.1.1 Series-1 Laboratory Test Results with Ballast Aggregate

Plate load tests were conducted for a control test without geogrid and geogrid stabilized tests having one layer of an extruded triaxial polypropylene geogrid. Cyclic loads and unloads of different load intensities were applied and corresponding surface deformations monitored. The results for each repetition of applied load intensity were averaged to obtain a representative value for use in modeling. Lack of confinement at the aggregate surface resulted in slight heave occurring in a zone within approximately 180 mm to 254 mm relative to the load plate centerline (or 27.5 mm to 101 mm beyond the load plate imprint) and may be attributed to particle rearrangement. Illustrated in Figure 3(a) are the measured results for Series-1 control test and the stabilized aggregate layer using geogrid. As expected, the geogrid stabilized layer exhibited less vertical deformation than the unstabilized aggregate layer of the control, and the trend of reducing deformation increased with higher applied stress for the test conditions used.

3.1.2 Series-2 Laboratory Test Results with Fireglass Aggregate

Shown in Figure 3(b) are the results from plate load tests with the fireglass aggregate material. The complete load-unload cycles are shown for the control and geogrid stabilized tests. It is seen that vertical deformation corresponding to the load and unload segments for the control test were higher than those for the multiaxial geogrid test. The maximum nominal applied stress of 380 kPa corresponds with vertical deformation of 79 mm and 47.8 mm for the control and geogrid stabilized tests, respectively, and relates to an exhibited difference between them of 31 mm or a factor of 1.65. The unload phase with minimum average applied stress of 2.64 kPa for the control and geogrid stabilized tests showed a vertical deformation of 18 mm and 6.4 mm, respectively, with a difference of 1.7 mm or a factor of 2.8. It is noteworthy that Series-2 tests using the fireglass aggregate exhibited relatively more vertical deformation than corresponding Series-1 testing with ballast aggregate. Comparisons of control test results shows the fireglass aggregate to have undergone 1.5 times more deformation for the loading phase and 2 times more deformation for the unloading phase. Similarly, the triaxial geogrid stabilized tests with fireglass aggregate exhibited 1.3 times and 1.4 times more deformation during loading and unloading phases, respectively. Notwithstanding using relatively simplistic load testing methods for the same geogrid material and aggregate layer thickness, the test results verify that the type of aggregate material used can manifest significant differences in vertical deformation.

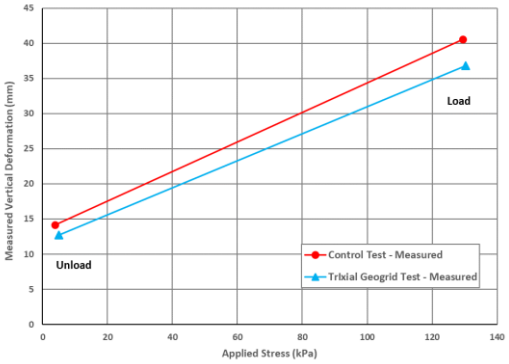

(a) Series-1 ballast aggregate tests

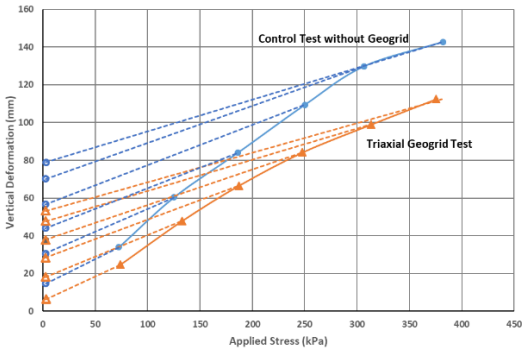

(b) Series-2 fireglass aggregate tests

Figure 3. Average applied stress and measured surface deformation for specific load-unload cycles

3.1.3 Series-2 Laboratory Testing and Lateral Confinement Measurement

Several laboratory plate load tests with fireglass included placing five 9-mm metal cubes at nominal vertical distances of 4 mm above the geogrid. The relative location of each cube is shown in Figure 4. The horizontal locations

of the metal cubes correspond to the centerline of the load plate (x,y coordinates of 0 mm, 4 mm above geogrid), just outside the load plate perimeter (x,y coordinates of 178 mm, 4 mm above geogrid), and about 1.5 times the radius of the load plate (x,y coordinates of 254 mm, 4 mm). At the conclusion of each test, a metal detector was used to identify the relative horizontal position of each cube, followed by careful exhumation to verify the final horizontal and vertical positions of the cubes. Results of the relative horizontal movement of the metal cubes is shown in Figure 5. Clearly the load test conducted with the multiaxial geogrid shows significantly less horizontal movement of the metal cubes compared to the control test without geogrid. The lesser amount of horizontal movement exhibited for the geogrid stabilized test indicates successful lateral confinement of the aggregate layer near the geogrid. It is expected that the extent of lateral confinement of the aggregate will diminish as the vertical distance from the geogrid increases, however increasing the vertical distance of the cube from the plane of the geogrid was not included in this testing program.

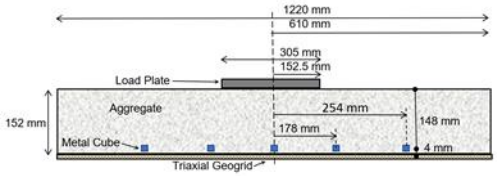

Figure 4. Schematic representation depicting relative locations of metal cubes above the geogrid

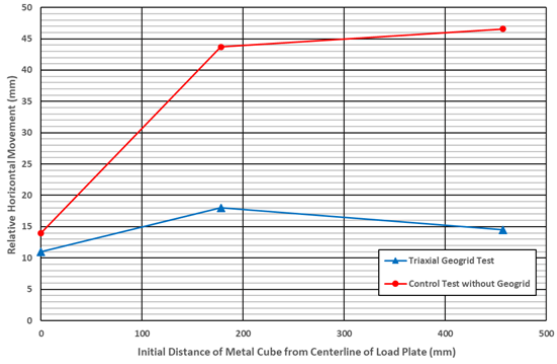

Figure 5. Initial location and relative horizontal movement of metal cubes embedded in fireglass aggregate material

4. NUMERICAL MODELING VERTICAL DEFORMATION

To garner a first approximation for numerical modeling using FEM, whether with or without geogrid in the testing application, it is highly desirable to initially use the basic Mohr-Coulomb (MC) model for the soil material. The MC model is a linear elastic perfectly plastic condition exhibiting linear elastic behavior until failure. With the MC model, one stiffness value is used for all soil behavior and dilatancy is only mobilized at failure. This model is generally familiar to most geotechnical engineers and requires only basic material parameters to be entered.

Fortunately, most FEM software (PLAXIS 2D and 3D was used) provides more advanced soil models to address some of the complexities discussed previously. To this end, the advanced hardening soil (HS) model can be used whereby the yield surface of the hardening plasticity model is not fixed in principal stress space but can expand due to plastic straining. In the HS model, plasticity occurs before failure criterion is reached and is therefore more realistic. The HS soil model accounts for stress-dependency of stiffness moduli; different moduli can be used for load-unload conditions and dilatancy is mobilized before failure is reached. Soil will show a decreasing stiffness when irreversible plastic strains develop. The HS model can give a better prediction of displacements than the MC model and especially when shear is dominant or unload/reloading behavior is important.

4.1 Numerical Modeling Series-1 Laboratory Tests with Ballast Aggregate

4.1.1 Selection of Soil Parameters for Series-1 Laboratory Testing

Soil parameters were selected by correlations found in the literature (Brinkgreve et el., 2010; Lees, 2012; Leng and Gabr, 2005) and supplemented by numerous calculation attempts. The ballast parameters and geogrid element parameters used are shown in Table 1. Note the geogrid parameters are representative for a biaxial geogrid and herein lies a problem since these parameters are not applicable to multiaxial geogrids used in the plate load tests. For comparative purposes of the model results, basic soil parameters used in the MC model were also used in the HS model. Although parametric determination is difficult, a possible good estimation based on limited data will generally give better results than using the MC model (Finno, R., 2014).

Table 1. Ballast aggregate material model and geogrid element parameters

Parameter	Units	Value
Soil Weight, γ_{unsat}	(kN/m^3)	18.7
Soil Weight, γ_{sat}	(kN/m^3)	18.7
Young's modulus, E'	(kPa)	430.9
Poisson's ratio, v'	-	0.33
Cohesion, c'	(kPa)	2.39
Friction angle, φ'	°	40
Dilatency angle, ψ	°	0
E'_{inc}	(kPa)	144
E_{50}	(kPa)	1389
E_{oed}	(kPa)	1374
E_{ur}	(kPa)	2777
m	-	0.5
v_u	-	0.2
Geogrid axial stiffness EA[1]	(kg/m)	2000[1]

[1]Representative of biaxial geogrid; parameter is not applicable to multiaxial geogrid

4.1.2 Numerical Modeling Results for Ballast Aggregate Series-1 Testing

Numerical analyses for the vertical deformation tests using ballast aggregate are based on a 3D PLAXIS model. Recall usage of interface elements on the ballast side of the geogrid will not exhibit changes to the calculated vertical deformation and this result is not realistic. The geogrid contributes to adding stiffness and lateral particle confinement to the ballast layer above it. Limitations of the interface element strength do not allow an increase in the tensile stiffness of the aggregate layer above the geogrid, nor does the element allow for a much larger zone of interfacial thickness.

Depicted in Figure 6(a) are the results of numerical analyses using MC and HS soil models for the Control test and Figure 6(b) shows the results for the multiaxial geogrid stabilized test. As expected, increasing model complexity results in calculated vertical deformations more closely matching the actual surface vertical deformations. Clearly, the closer match between calculated and actual surface vertical deformation requires consideration of more complex soil response to loading and unloading behavioral phenomena as indicated by the variance in predictions and especially for the unloading phase. For all tests and soil models used, the calculated vertical deformation for unloading was problematic and overall is lacking realism in prediction or verification of laboratory testing results.

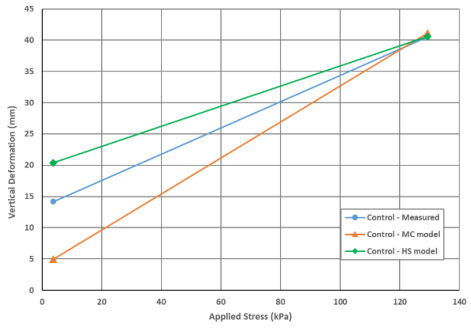

(a) Control test without geogrid

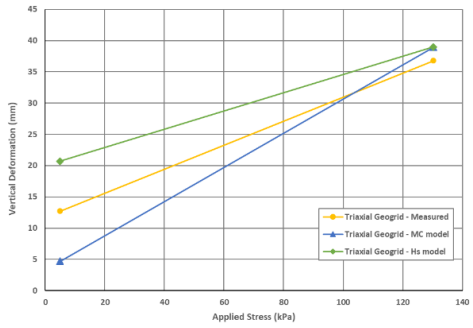

(b) Triaxial geogrid stabilized test

Figure 6. Deformation results for FEM modeling and actual measured laboratory test results for Series-1 tests using ballast aggregate

4.2 Numerical Modeling Series-2 Laboratory Tests with Fireglass Aggregate

4.2.1 Soil Parameters for Series-2 Testing

Soil parameters were selected based on consideration of typical values for a natural aggregate material simulated by the fireglass. Parameters for the other materials used in the tests remained the same as those used in Series-1 testing to allow relative comparisons between testing series results. The fireglass aggregate parameters used and geogrid parameter (for planar element purposes) are shown in Table 2. The MC soil model was used for both the Control test and the geogrid stabilized test.

Table 2. Fireglass aggregate material model and geogrid element parameters

Parameter	Units	Value
Soil Weight, γ_{unsat}	(kN/m^3)	18
Soil Weight, γ_{sat}	(kN/m^3)	18
Young's modulus, E'	(kPa)	500
Poisson's ratio, v'	-	0.4
Cohesion, c'	(kPa)	100
Friction angle, φ'	°	35
Dilatency angle, ψ	°	5
Geogrid axial stiffness EA[1]	(kg/m)	2000[1]

[1]Representative of biaxial geogrid; parameter is not applicable to multiaxial geogrid

Unique to this test series was usage of the composite material TSSM model that does not use the traditional geogrid planar element. This soil model is a constitutive linear elastic perfectly plastic composite model. The composite material is described by a curved soil strength envelope that has been implemented into a FEM program module to produce accurate simulations of triaxial compression tests on a geogrid-stabilized granular soil (Lees and Clausen, 2018). This composite material model replaces inserting the traditional geogrid element into the application geometry. The geogrid stabilized soil is modeled as one material rather than soil and geogrid separately. Unlike the traditional planar geogrid element, the geogrid itself is not modeled but rather the effect of geogrid on the soil around it. Development of this composite geogrid-soil model and technical background can be found in the literature (Lees, A.S., 2019; Lees, A.S., 2017a and 2017b). Estimations and modifications based on numerous calculations were used to determine the best fit soil parameters since the materials used in testing were not used in triaxial compression test simulations on stabilized soil. Soil parameters used for the composite geogrid stabilized soil are shown in Table 3.

Table 3. Fireglass aggregate material parameters used in composite soil model

Parameter	Units	Value
Soil Weight, γ_{unsat}	(kN/m^3)	18
Soil Weight, γ_{sat}	(kN/m^3)	18
Young's modulus, E' - MC	(kPa)	500
Young's modulus, E' - TSSM	(kPa)	1425
Poisson's ratio, v'	-	0.4
Cohesion, c'	(kPa)	100
Friction angle, φ'	°	35
Dilatency angle, ψ	°	5

4.2.2 Numerical Modeling Results for Fireglass Aggregate Series-2 Testing

FEM modeling of load-deformation results for fireglass aggregate testing was performed using PLAXIS 2D. The Control test was modeled using the traditional MC soil model. The geogrid stabilized test was modeled using the MC soil model with the traditional geogrid element and also with the TSSM composite material model. FEM modeling results for fireglass aggregate testing are illustrated in Figure 7 – Figure 9. Comparison of FEM soil model predictions and verifications are shown in Figure 10.

Comparing the FEM plots of total deformation, it is shown that the addition of geogrid causes a load spreading mechanism to decrease vertical deformation. However, the performance of the geogrid may be under-or-over predicted by the soil model and use of the geogrid planar element available in FEM software. The problem of under-predicting geogrid performance can be significantly lessened by using a geogrid composite material instead of modeling the geogrid and the adjacent soil independently. Figure 10 clearly illustrates verification of the performance of load-deformation prediction ability of the geogrid composite soil model compared to other traditional models.

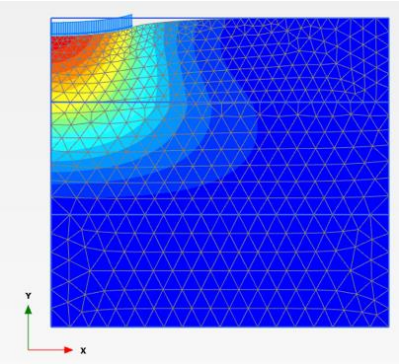

Figure 7. Control test without geogrid stabilization. Predicted total displacements = 0.03308 m (plot is scaled up 0.5 times) for load phase and unloading phase predicted total displacements = 0.00156 m. Actual displacements were 0.0339 m and 0.0147 m for the load and unload phases, respectively.

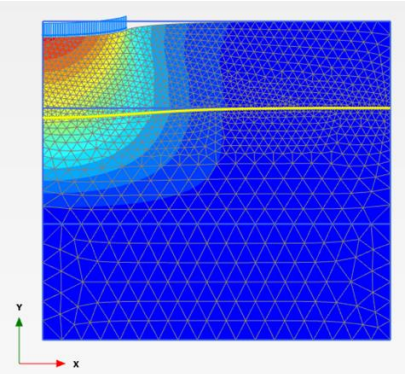

Figure 8. Geogrid stabilized test with MC soil model and geogrid element. Total displacement max value = 0.02828 m (plot is scaled up 0.5 times) for load phase and unloading phase predicted total displacements = 0.00144 m. Actual displacements were 0.0248 m and 0.0064 m for the load and unload phases, respectively.

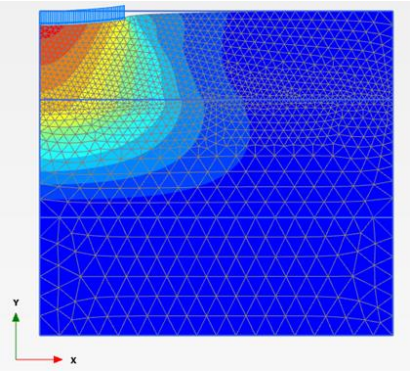

Figure 9. Geogrid stabilized test with TSSM soil model. Total displacement max value = 0.02484 m (plot is scaled up 0.5 times) for load phase and unload model predicted total displacements = 0.00593 m. Actual displacements were 0.0248 m and 0.0064 m for the load and unload phases, respectively.

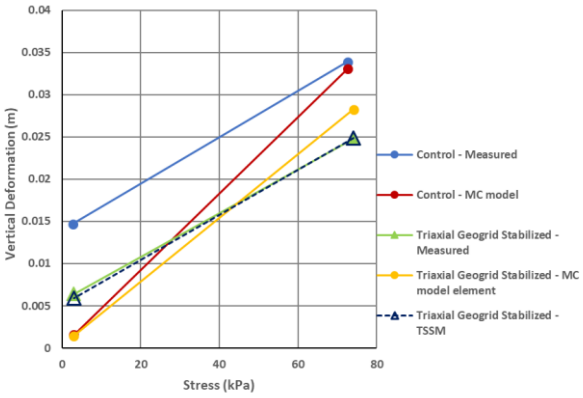

Figure 10. FEM predictions of load-deformation results and verification with laboratory test measured results

5. CONCLUSIONS

Vertical deformation results calculated by FEM using MC and HS soil models with and without multiaxial geogrid are compared with results from simple laboratory plate load tests. In this study, using an advanced soil model such as HS better estimates the vertical surface deformation, however the unload deformation did not satisfactorily compare with actual test results. Geogrid-aggregate interaction is key to modeling soil stabilization. In this study, using the planar geogrid element and the interface element does not realistically model the effect of the geogrid for increasing the tensile stiffness of the overlying aggregate layer, nor do the elements allow for a much larger zone of interfacial thickness. Accordingly, a composite material model, such as TSSM used in this study, for the geogrid stabilized soil can satisfactorily verify prediction of the actual deformation measured in the laboratory tests. Laboratory plate load tests were also used to verify the effective lateral confinement and aggregate interlock provided by a multiaxial geogrid by measuring the relative horizontal movement of metallic cubes post-test.

6. ACKNOWLEDGEMENT

The authors would like to greatfully acknowledge Lynn Cassidy who provided assistance with the in-house laboratory testing.

7. REFERENCES

Brinkgreve, R.B.J. and Engin, E. 2013. Validation of geotechnical finite element analysis, *18th International Conference on Soil Mechanics and Geotechnical Engineering*, Paris, 677-682.

Bussert, F. and Cavanaugh, J. 2010. Recent research and future implications of the actual behavior of geogrids in reinforced soil, *ASCE Earth Retention Conference* (ER2010), Washington, USA, 460-477.

Dong, Y.L., Han, J., and Bai, X.H. 2010a. Numerical analysis of tensile behavior of geogrids with rectangular and triangular apertures, *Geotextiles and Geomembranes*, 29: 83-91.

Finno, R. 2014. The hardening soil model and parameter selection, *Computational Geotechnics Course*, PLAXIS.

Gabr, M.A., Dodson, R., and Collin, J.G. 1998. A study of stress distribution in geogrid-reinforced sand, *GeoShanghai International Conference*, China, ASCE 76: 62-76.

Giroud, J.P. 2009. An assessment of the use of geogrids in unpaved roads and unpaved areas, *Jubilee Symposium on Polymer Geogrid Reinforcement*, London, 23-36.

Giroud, J.P. and Han, J. 2016a. Part I: Mechanisms governing the performance of unpaved roads incorporating geosynthetics, *Geosynthetics*, Feb 2016.

Giroud, J.P. and Han, J. 2016b. Part II: Mechanisms governing the performance of unpaved roads incorporating geosynthetics, *Geosynthetics*, Apr 2016.

Guido, V.A., Knueppel, J.D., and Sweeny, M.A. 1987. Plate loading tests on geogrid-reinforced earth slabs, *Geosynthetics 87 Conference*, New Orleans, 216-225.

Jersey, S.R. and Tingle, J.S. 2009. Cyclic plate testing of geogrid-reinforced highway pavements, USACE ERDC/GSL TR-09036, Vicksburg, MS.

Lees, A. 2012. *Obtaining parameters for geotechnical analysis*, NAVFEMS.

Lees, A. 2017a. Bearing capacity of a stabilized granular layer on clay subgrade, *10th International Conference on Bearing Capacity of Roads, Railways and Airfields*, Taylor and Francis Group, London, 1135-1142.

Lees, A. 2017b. Simulation of geogrid stabilization by finite element analysis, *International Conference on Soil Mechanics and Geotechnical Engineering*, Seoul, 1377-1380.

Lees, A. 2019. The bearing capacity of a granular layer on clay, *ICE Virtual Library, ICE Publishing, Group of Thomas Telford Ltd.*, accepted manuscript doi: 10.1680/jgeen.18.00116.

Leng, L. and Gabr, M.A. 2005. Numerical analysis of stress-deformation response in reinforced unpaved road sections, *Geosynthetics International*, 12, 5:111-119.

Milligan, G.W.E., Jewell, R.A., Houlsby, G.T., and Burd, H.J. 1989. A new approach to the design of unpaved roads - Part I, *Ground Engineering*, 22, Apr: 25-29.